Functional impact of a congenital stationary night blindness type 2 mutation depends on subunit composition of $Ca_v1.4$ Ca^{2+} channels

Received for publication, April 30, 2020, and in revised form, September 17, 2020 Published, Papers in Press, October 8, 2020, DOI 10.1074/jbc.RA120.014138

Brittany Williams[1,2], **Josue A. Lopez**[1], **J. Wesley Maddox**[1], **and Amy Lee**[1,*]

From the [1]*Departments of Molecular Physiology and Biophysics, Otolaryngology Head-Neck Surgery, and Neurology, Iowa Neuroscience Institute, Pappajohn Biomedical Institute and the* [2]*Interdisciplinary Graduate Program in Neuroscience, University of Iowa, Iowa City, Iowa, USA*

Edited by Michael J. Shipston

Voltage-gated Ca_v1 and Ca_v2 Ca^{2+} channels are comprised of a pore-forming α_1 subunit ($Ca_v1.1$-1.4, $Ca_v2.1$-2.3) and auxiliary β ($\beta_{1\text{-}4}$) and $\alpha_2\delta$ ($\alpha_2\delta{-}1{-}4$) subunits. The properties of these channels vary with distinct combinations of Ca_v subunits and alternative splicing of the encoding transcripts. Therefore, the impact of disease-causing mutations affecting these channels may depend on the identities of Ca_v subunits and splice variants. Here, we analyzed the effects of a congenital stationary night blindness type 2 (CSNB2)-causing mutation, I745T (IT), in $Ca_v1.4$ channels typical of those in human retina: $Ca_v1.4$ splice variants with or without exon 47 ($Ca_v1.4$+ex47 and $Ca_v1.4\Delta$ex47, respectively), and the auxiliary subunits, β_{2X13} and $\alpha_2\delta$-4. We find that IT caused both $Ca_v1.4$ splice variants to activate at significantly more negative voltages and with slower deactivation kinetics than the corresponding WT channels. These effects of the IT mutation, along with unexpected alterations in ion selectivity, were generally larger in channels lacking exon 47. The weaker ion selectivity caused by IT led to hyperpolarizing shifts in the reversal potential and large outward currents that were evident in channels containing the auxiliary subunits β_{2X13} and $\alpha_2\delta$-4 but not in those with β_{2A} and $\alpha_2\delta$-1. We conclude that the IT mutation stabilizes channel opening and alters ion selectivity of $Ca_v1.4$ in a manner that is strengthened by exclusion of exon 47 and inclusion of β_{2X13} and $\alpha_2\delta$-4. Our results reveal complex actions of IT in modifying the properties of $Ca_v1.4$ channels, which may influence the pathological consequences of this mutation in retinal photoreceptors.

Voltage-gated Ca^{2+} (Ca_v) channels are comprised of a pore-forming α_1 subunit and two auxiliary subunits, β and $\alpha_2\delta$ (reviewed in Ref. 1). The α_1 subunit is comprised of 4 homologous domains (I-IV), each containing 6 alpha-helical transmembrane-spanning segments (S1–S6); the S1–S4 segments form a voltage-sensing domain, and S5–S6 forms the pore (2). In contrast to the diverse complement of Ca_v channels expressed in many neurons, the pore-forming α_{1F} subunit (referred to as $Ca_v1.4$ from here on), encoded by the *Cacna1f* gene, appears to be the major Ca_v subtype localized in the synaptic terminals of photoreceptors in the retina (3, 4) where it co-assembles with β_2 and $\alpha_2\delta$-4 subunits (5). Within photoreceptor synaptic terminals, $Ca_v1.4$ channels are activated at the relatively depolarized voltage of these cells in darkness, causing the tonic release of glutamate. At the sign-inverting synapse formed between photoreceptors and depolarizing bipolar cells, the termination of $Ca_v1.4$-dependent glutamate release by light stimuli enables disinhibition of a nonselective cation channel, initiating excitation of the ON pathway in the retina (6, 7). Thus, the voltage-dependent properties of $Ca_v1.4$ are critical parameters for controlling the dynamic range of visual signaling.

More than 140 mutations in *Cacna1f* have been identified and are linked to vision disorders including congenital stationary night blindness type 2 (CSNB2) (reviewed in Ref. 8). The sequelae of these mutations are not entirely clear because, when analyzed in heterologous expression systems, they can weaken, enhance, or have no impact on the function of $Ca_v1.4$ (9–13). Understanding the pathological consequences of CSNB2 mutations is complicated by the functional diversity of retinal $Ca_v1.4$ conferred in part by alternative splicing of the pre-mRNAs corresponding to each subunit (5, 14–16). The β_2 variant that is most highly expressed in human retina contains an alternatively spliced exon 7B (β_{2X13}) and causes stronger voltage-dependent inactivation of $Ca_v1.4$ than β_2 variants with exon 7A (β_{2A}) (5). The $Ca_v1.4$ α_1 pre-mRNA also undergoes alternative splicing, particularly in the sequence encoding the large cytoplasmic C-terminal domain (15, 16). We previously characterized a $Ca_v1.4$ variant lacking exon 47 ($Ca_v1.4\Delta$ex47) that is highly expressed in human retina (16). Exon 47 encodes a portion of a C-terminal modulatory domain (CTM) in $Ca_v1.4$ that suppresses Ca^{2+}-dependent inactivation (CDI) and causes depolarizing shifts in the voltage-dependence of activation (10, 17). When expressed in a human embryonic kidney cell line (HEK293T), $Ca_v1.4\Delta$ex47 exhibits more negative activation thresholds and stronger CDI than $Ca_v1.4$ variants containing exon 47 ($Ca_v1.4$+ex47) (16, 18).

Studies investigating the electrophysiological consequences of *Cacna1f* mutations have focused on the $Ca_v1.4$+ex47 variant coexpressed with auxiliary subunits other than β_{2X13} and $\alpha_2\delta$-4 (9–13). Alternative splicing can affect the severity of disease-causing mutations in Ca_v channel genes (19). Thus, analysis of *Cacna1f* mutations in the context of $Ca_v1.4$

* For correspondence: Amy Lee, amy-lee@uiowa.edu.
Present address for Brittany Williams: Department of Cell Biology & Physiology, Carolina Institute for Developmental Disabilities, and Neuroscience Center, University of North Carolina, Chapel Hill, North Carolina USA.

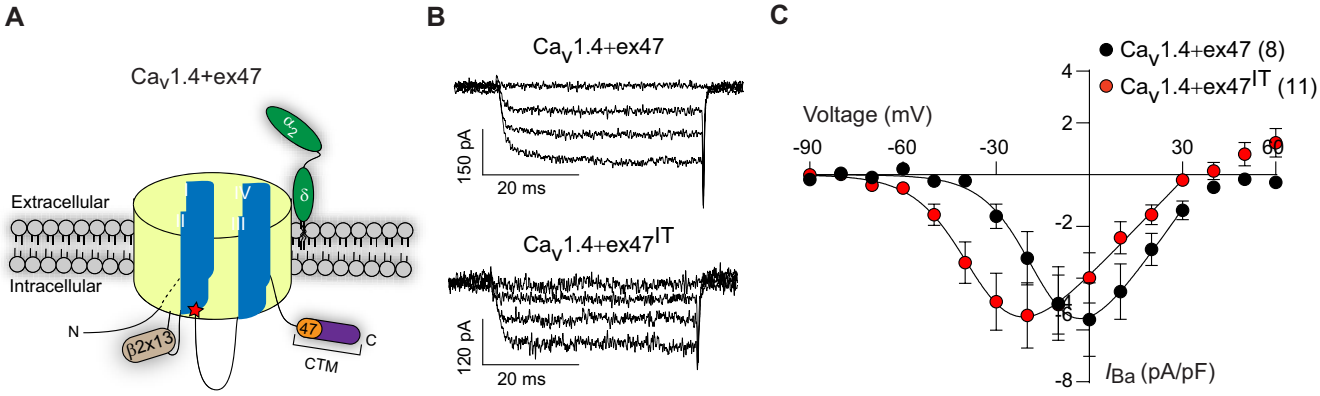

Figure 1. IT enhances voltage-dependence of activation of $Ca_v1.4$+ex47. *A,* schematic of $Ca_v1.4$ pore-forming α_1 subunit with 4 transmembrane spanning domains (I-IV; *blue*), and β_{2X13} (*tan*) and $\alpha_2\delta$-4 (*green*) subunits. The CTM of $Ca_v1.4$ (*purple*) contains exon 47 (*orange*). The *red star* illustrates the location of IT in domain II. *B,* representative I_{Ba} family of traces for $Ca_v1.4$+ex47 or $Ca_v1.4$+ex47^{IT}. *C,* I-V plots for I_{Ba} current density (pA/pF) in cells transfected with $Ca_v1.4$+ex47 (*black*) or $Ca_v1.4$+ex47^{IT} (*red*). I_{Ba} was evoked by 50-ms pulses from −100 mV to various voltages. Here and in all graphs of electrophysiological data, *parentheses* indicate number of cells, and *symbols* and *error bars* represent mean ± S.E., respectively.

variants expressed in photoreceptors in human retina is necessary for understanding the visual phenotypes associated with such mutations.

Here, we investigated the effects of a CSNB2-causing mutation on the properties of $Ca_v1.4$+ex47 and $Ca_v1.4\Delta$ex47 channels containing β_{2X13} and $\alpha_2\delta$-4. The mutation results in the replacement of isoleucine 745 with a threonine (IT) in the S6 helix of domain 2 (IIS6, Fig. 1*A*). In $Ca_v1.4$+ex47 coexpressed with $\alpha_2\delta$-1 and β_3 or β_2, the IT mutation causes a large hyperpolarizing shift (>30 mV) in the voltage-dependence of activation (12). Our results indicate that, when coexpressed with β_{2X13} and $\alpha_2\delta$-4, $Ca_v1.4$+ex47 channels bearing the IT mutation ($Ca_v1.4$+ex47^{IT}) show hyperpolarized activation voltages compared with wild-type (WT) channels. The gain-of function effect is more severe for $Ca_v1.4\Delta$ex47 channels with the IT mutation ($Ca_v1.4\Delta$ex47^{IT}), which showed more negative activation thresholds and slower deactivation kinetics than $Ca_v1.4$+ex47^{IT}. An unexpected finding is that IT alters the ion selectivity of both $Ca_v1.4$ splice variants in a manner that varies with the identity of the $\alpha_2\delta$ subunit. Our findings highlight the importance of splice variation and auxiliary subunit composition as potential modifiers of disease-causing mutations affecting Ca_v channels.

Results

IT mutation enhances activation and slows deactivation of $Ca_v1.4$+ex47

Exon 47 resides in the CTM of $Ca_v1.4$ (Fig. 1*A*); deletion of this exon, like the IT mutation, causes a large negative shift in the voltage dependence of channel activation (16, 18). Thus, the effect of IT on $Ca_v1.4$ activation could be additive, or alternatively, could be occluded by exon 47 deletion. To distinguish between these possibilities, we compared the activation properties of Ba^{2+} currents (I_{Ba}) mediated by $Ca_v1.4$+ex47 and $Ca_v1.4\Delta$ex47, and the corresponding IT mutant channels, in transfected HEK293T cells. Ba^{2+} rather than Ca^{2+} was used as the charge carrier to minimize the complicating effects of CDI which, whereas negligible in $Ca_v1.4$+ex47, is prominent in $Ca_v1.4\Delta$ex47 (18). Because previous analyses of $Ca_v1.4$+ex47^{IT} were performed primarily with β_3 or β_{2a}, and $\alpha_2\delta$-1 (12), we first characterized the effect of IT on $Ca_v1.4$+ex47 coexpressed with auxiliary subunits representative of $Ca_v1.4$ complexes in the retina (*i.e.* β_{2X13} and $\alpha_2\delta$-4 (5)). Although there was no effect of IT on the slope factor (k), Boltzmann fits of current-voltage (I-V) plots showed that the half-maximal voltage of activation (V_h) of $Ca_v1.4$+ex47^{IT} was significantly more negative than that of $Ca_v1.4$+ex47 (Fig. 1, *B* and *C*, Table 1).

Exponential fits of the rising phase of the peak currents yielded time constants for activation (τ_{act}) that were significantly longer (Table 2) and with weaker voltage dependence for $Ca_v1.4$+ex47^{IT} (v = −50.3 mV) than for $Ca_v1.4$+ex47 (v = −26.9 mV; $F_{2,7}$ = 16.4, p = 0.002; Fig. 2, *A* and *B*). To analyze rates of channel closure, the time constant for deactivation (τ_{deact}) was obtained from exponential fits of the decay phase of the tail current evoked upon repolarization of the membrane voltage. τ_{deact} was significantly greater at the most positive repolarization voltage tested (-60 mV, Table 2) and the voltage-dependence of τ_{deact} was significantly steeper for $Ca_v1.4$+ex47^{IT} (v = 43.1 mV) than for $Ca_v1.4$+ex47 (v = 169.9 mV; $F_{2,22}$ = 59.2, $p < 0.0001$; Fig. 2, *C* and *D*). Thus, as has been shown for $Ca_v1.2$ channels bearing the analogous IT mutation (20), IT slows the activation and deactivation of $Ca_v1.4$ containing exon 47 in a highly voltage-dependent manner.

Deletion of exon 47 augments effects of the IT mutation on voltage-dependent gating of $Ca_v1.4$

We next investigated how deletion of exon 47 affects the impact of the IT mutation (Fig. 3*A*). As for $Ca_v1.4$+ex47 (Fig. 1*C*), IT caused a negative shift in V_h for $Ca_v1.4\Delta$ex47 (Fig. 3, *B* and *C*, Table 1). The net hyperpolarizing effect of IT (ΔV_h) was not significantly different between $Ca_v1.4$+ex47 (median ΔV_h= 19.9 mV, n = 11) and $Ca_v1.4\Delta$ex47 (median ΔV_h= 18.9 mV, n = 8; Mann-Whitney U = 44, $p > 0.999$). However, the additive effects of the IT mutation and deletion of exon 47 resulted in an extremely negative activation threshold of $Ca_v1.4\Delta$ex47^{IT} (~ −70 mV, Fig. 3*C*). Moreover, IT enhanced rather than

Table 1

Parameters from I–V relationships of $Ca_v1.4$+ex47 and $Ca_v1.4\Delta$ex47 with or without IT mutation

V_h, k, E_{rev}, and peak I_{Ba} values (mean ± S.E.) were determined from Boltzmann fits of the I-V data in Figs. 1, 3, and 9 and as described under "Experimental procedures."

	Peak I_{Ba} (pA/pF)	p Value	V_h (mV)	p Value	k	p Value	E_{rev} (mV)	p Value
$Ca_v1.4$+ex47 + β_{2x13} + $\alpha_2\delta$-4	−5.6 ± 1.4	–	−8.6 ± 0.4	–	−6.2 ± 1.6	–	58.3 ± 3.7	–
$Ca_v1.4$+ex47^{IT} + β_{2x13} + $\alpha_2\delta$-4	−5.3 ± 1.2	0.904[a]	−28.5 ± 2.0	<0.0001[a]	−8.5 ± 1.2	0.253[b]	37.1 ± 3.7	<0.0001[a]
$Ca_v1.4\Delta$ex47 + β_{2x13} + $\alpha_2\delta$-4	−10.5 ± 1.9	–	−24.8 ± 1.3	–	−6.6 ± 0.4	–	54.3 ± 1.5	v
$Ca_v1.4\Delta$ex47^{IT} + β_{2x13} + $\alpha_2\delta$-4	−2.6 ± 0.4	0.002[b]	−43.7 ± 2.1	<0.0001[b]	−11.2 ± 1.0	<0.001[b]	16.7 ± 5.0	<0.0001[a]
$Ca_v1.4$+ex47 + β_{2A} + $\alpha_2\delta$-1	−11.2 ± 2.0	–	−2.7 ± 1.2	–	−7.1 ± 0.2	–	52.7 ± 0.8	–
$Ca_v1.4$+ex47^{IT} + β_{2A} + $\alpha_2\delta$-1	−9.2 ± 3.0	0.581[b]	−28.3 ± 2.0	<0.0001[b]	−7.4 ± 1.1	0.527[a]	50.1 ± 2.4	0.237[b]
$Ca_v1.4\Delta$ex47 + β_{2A} + $\alpha_2\delta$-1	−17.8 ± 0.9	–	−19.2 ± 0.5	–	−4.6 ± 0.8	–	50.4 ± 3.2	–
$Ca_v1.4\Delta$ex47^{IT} + β_{2A} + $\alpha_2\delta$-1	−0.6 ± 0.1	0.082[b]	−36.1 ± 2.5	0.003[b]	−7.7 ± 0.5	0.009[b]	41.0 ± 3.2	0.121[b]

[a] Mann-Whitney test.
[b] Student's t test.

Table 2

Time constants for activation and deactivation of $Ca_v1.4$+ex47 and $Ca_v1.4\Delta$ex47 with or without IT mutation

τ_{act} was obtained from single exponential fits of the rising phase of currents evoked by the voltages indicated in parentheses. τ_{deact} was obtained from single exponential fits of the rising phase of currents evoked upon depolarization from 10-ms steps to voltages evoking peak inward I_{Ba} indicated in parentheses and repolarization to −60 mV.

Channel	τ_{act} (ms)	p Value	τ_{deact} (ms)	p-Value
$Ca_v1.4$+ex47 + β_{2x13} + $\alpha_2\delta$-4	1.8 ± 0.2 (0 mV)	–	4.4 ± 0.8 (0 mV)	–
$Ca_v1.4$+ex47^{IT} + β_{2x13} + $\alpha_2\delta$-4	2.8 ± 0.2 (−20 mV)	0.019[a]	14.2 ± 1.8 (−20 mV)	<0.001[a]
$Ca_v1.4\Delta$ex47 + β_{2x13} + $\alpha_2\delta$-4	2.0 ± 0.2 (−10 mV)	–	3.1 ± 0.3 (−10 mV)	–
$Ca_v1.4\Delta$ex47^{IT} + β_{2x13} + $\alpha_2\delta$-4	2.5 ± 0.4 (−30 mV)	0.343[a]	37 ± 9.7 (−30 mV)	0.004[b]

[a] Student's t test.
[b] Mann-Whitney test.

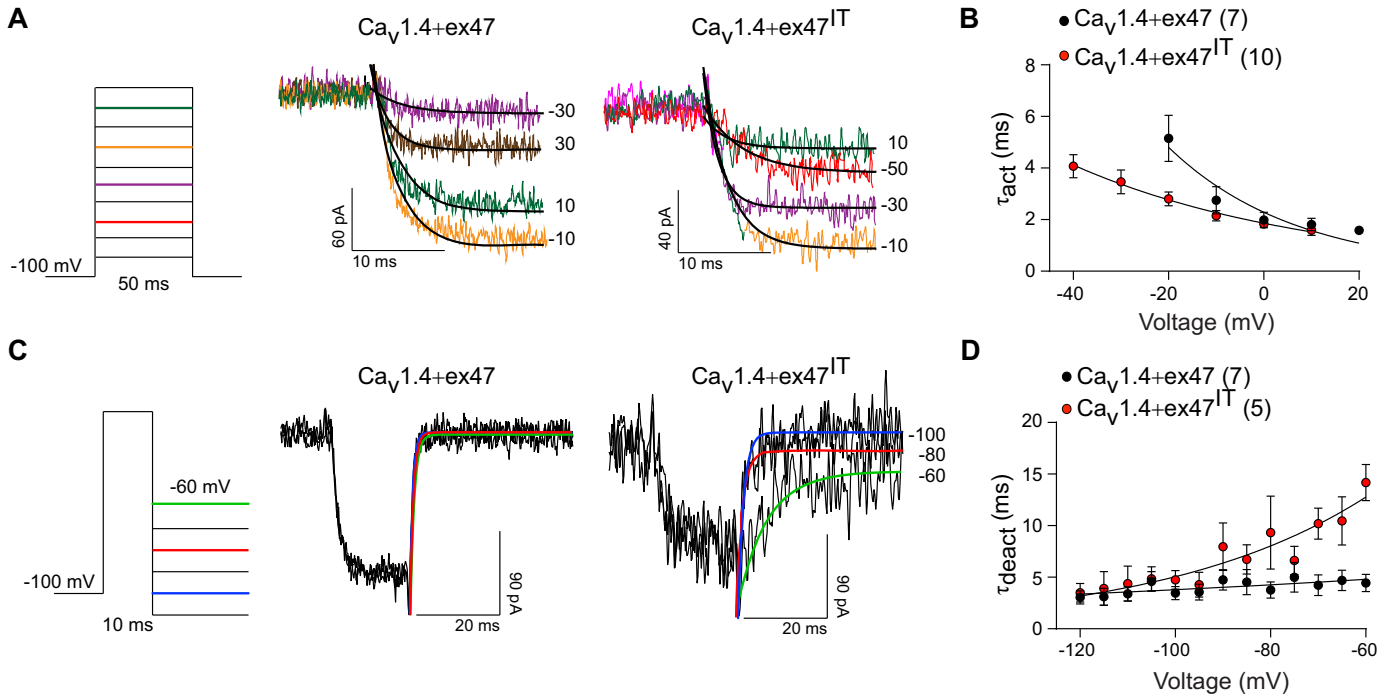

Figure 2. IT alters kinetics of activation and deactivation for $Ca_v1.4$+ex47. *A*, voltage protocol for measuring activation kinetics (*left*) and representative I_{Ba} family of traces (*right*). I_{Ba} was evoked by 50-ms pulses from −100 mV to various test voltages. Current traces are color-coded according to the depolarizations used to evoke them in voltage protocol. Exponential fits (*black* lines) are overlaid on corresponding current traces. *B*, activation time constants (τ_{act}) were obtained from exponential fits of I_{Ba} and plotted against test voltage in cells transfected with $Ca_v1.4$+ex47 (*black symbols*) or $Ca_v1.4$+ex47^{IT} (*red symbols*). *C*, voltage protocol for measuring deactivation kinetics (*left*) and representative family of I_{Ba} traces (*right*). Tail I_{Ba} was evoked by 10-ms pulses to voltages evoking peak inward I_{Ba} (see Table 2) followed by repolarizations to various voltages. Exponential fits of tail I_{Ba} are color-coded according to the repolarization voltage used to evoke them in voltage protocol. *D*, deactivation time constants (τ_{deact}) were obtained from exponential fits of tail I_{Ba} and plotted against repolarization voltage in cells transfected with $Ca_v1.4$+ex47 (*black symbols*) or $Ca_v1.4$+ex47^{IT} (*red symbols*). In *B* and *D*, *solid lines* represent exponential fits of the averaged data. $Ca_v1.4$ variants were co-expressed with β_{2X13} and $\alpha_2\delta$-4.

weakened the voltage-dependence of τ_{act} in the absence of exon 47 (v = −21.4 mV for $Ca_v1.4\Delta$ex47^{IT} *versus* v = −33.4 mV for $Ca_v1.4\Delta$ex47; $F_{2,8}$ = 5.3, p = 0.03; Fig. 4, *A* and *B*).

Similar to its effects in the presence of exon 47 (Fig. 2, *C* and *D*), IT strengthened the voltage-dependence of τ_{deact} (v = 104.1 mV for $Ca_v1.4\Delta$ex47 *versus* v = 27.6 mV for $Ca_v1.4\Delta$ex47^{IT};

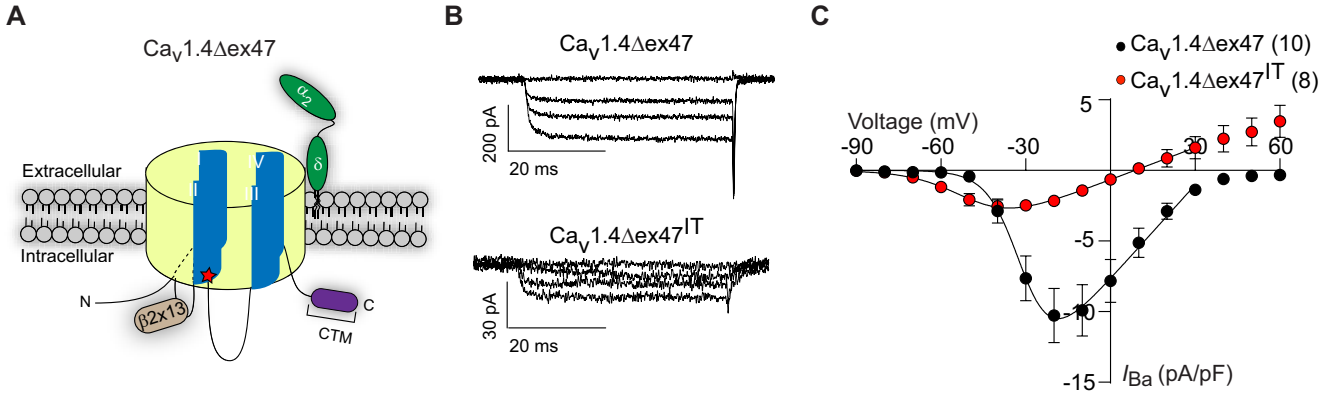

Figure 3. IT enhances voltage-dependence of activation of $Ca_v1.4\Delta ex47$ and decreases current density. *A–C*, same as described in the legend to Fig. 1, except for cells transfected with $Ca_v1.4\Delta ex47$ or $Ca_v1.4\Delta ex47^{IT}$ (*black* and *red symbols*, respectively in *C*).

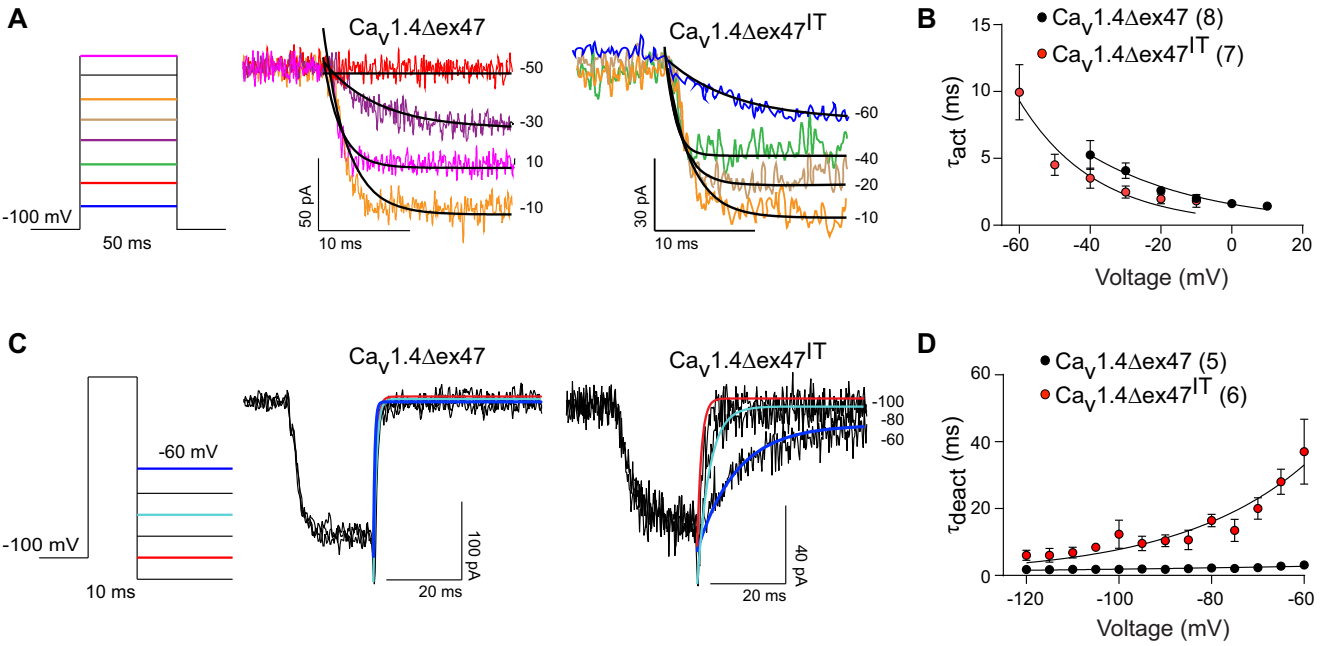

Figure 4. IT significantly alters the activation and deactivation kinetics of $Ca_v1.4\Delta ex47$. *A–D*, same as described in the legend to Fig. 2 except for cells transfected $Ca_v1.4\Delta ex47$ or $Ca_v1.4\Delta ex47^{IT}$ (*black* and *red symbols*, respectively in *B* and *D*).

$F_{2,22}$ = 151.6, $p < 0.0001$; Fig. 4, *C* and *D*). However, IT increased τ_{deact} more than 10-fold for $Ca_v1.4\Delta ex47$ *versus* ~4-fold for $Ca_v1.4$+ex47 upon repolarization to −60 mV (Table 2). These results indicate that deletion of exon 47 augments the gain-of-function effects of IT by modifying the kinetics and voltage-dependence of channel activation and deactivation.

Unique effects of IT on $Ca_v1.4\Delta ex47$

An effect of IT that was not reported previously was a reduction in current density, which was only seen in the absence of exon 47 (Figs. 1*C* and 3*C*, Table 1). We first tested the possibility that IT impaired the stability of the channel in ways that diminished overall levels of the $Ca_v1.4\Delta ex47$ protein. However, Western blots indicated similar levels of total channel protein in cells transfected with either $Ca_v1.4\Delta ex47$ or $Ca_v1.4\Delta ex47^{IT}$ (Fig. 5*A*). Moreover, biotinylation and streptavidin pulldown of cell-surface proteins revealed no significant difference in the levels of $Ca_v1.4\Delta ex47$ or $Ca_v1.4\Delta ex47^{IT}$ in the plasma membrane (Fig. 5*B*). Thus, impaired trafficking of the mutant channels to the cell surface was unlikely to be the major cause of the decrease in current density. A second unexpected effect of IT was an apparent decrease in ion selectivity based on the development of large outward currents at positive voltages and hyperpolarizing shift in the reversal potential (E_{rev}) (Figs. 1*C* and 3*C*, Table 1). The outward currents and median change in E_{rev} (ΔE_{rev}) were significantly larger for $Ca_v1.4\Delta ex47^{IT}$ (−37.2 mV, n = 8) than for $Ca_v1.4$+$ex47^{IT}$ (−16.6 mV, n = 11; Mann-Whitney U = 14, p = 0.01) relative to the corresponding WT channels. Therefore, we probed the underlying mechanism with an emphasis on $Ca_v1.4\Delta ex47$.

The nature of the outward currents was mysterious considering that the major intracellular cation in our recording solutions was $NMDG^+$ (*N*-methyl-D-glucamine), a large organic cation that does not permeate most voltage-gated ion channels. However, $Ca_v1.2$ and $Ca_v1.3$ are permeable to $NMDG^+$ under some conditions (21, 22). If IT enabled $NMDG^+$ efflux through

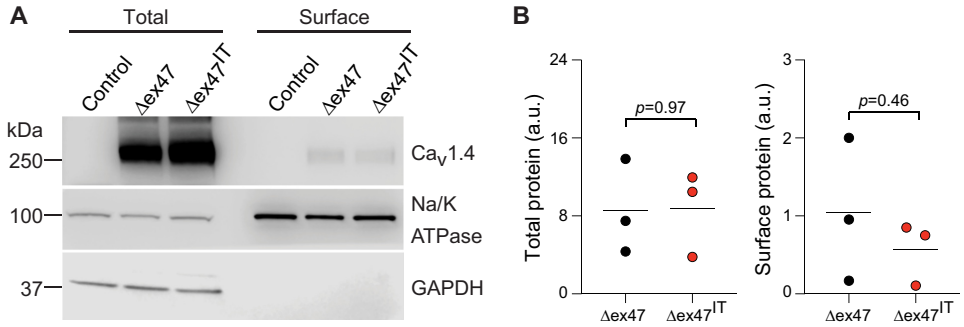

Figure 5. IT does not alter the expression levels or cell-surface density of $Ca_v1.4\Delta ex47$. *A,* representative Western blotting images of lysates from HEK293T cells that were untransfected (*Control*) or transfected with either $Ca_v1.4\Delta ex47$ (Δex47) or $Ca_v1.4\Delta ex47^{IT}$ ($\Delta ex47^{IT}$) as well as β_{2X13} and $\alpha_2\delta$−4. Blots were probed with antibodies against $Ca_v1.4$, Na/K-ATPase, or GAPDH. The percentage of lysates used for total protein (*left 3 lanes*) and biotinylated cell-surface proteins (*right 3 lanes*) were 10 and 90%, respectively. *B,* densitometric analysis of total and cell-surface $Ca_v1.4$ protein normalized to those for GAPDH and Na/K-ATPase, respectively. The use of these proteins as normalization controls was justified because there was no effect of transfection on their levels ($p = 0.84$ for GAPDH and $p = 0.99$ for Na/K-ATPase, both by analysis of variance). Each *point* represents result from an independent experiment. *Bars* represent mean; *p* values were determined by *t* test.

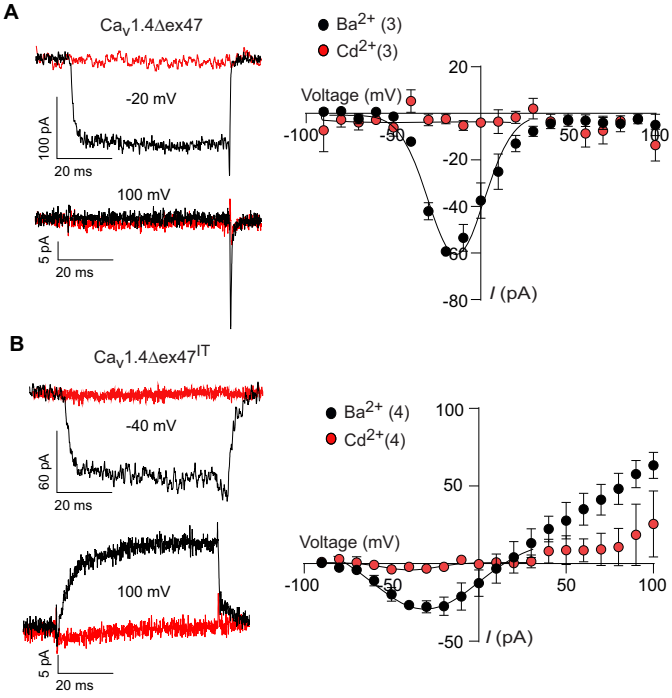

Figure 6. Cd^{2+} suppresses inward and outward currents in cells transfected with $Ca_v1.4\Delta ex47^{IT}$. *A* and *B,* representative traces (*left*) for I_{Ba} evoked by 50-ms pulses to the indicated voltages before (*black*) and after perfusion of extracellular solution containing Cd^{2+} (*red*; 100 μM). I-V plots (*right*) obtained before (Ba^{2+}, *black symbols*) and after (Cd^{2+}, *red symbols*) perfusion of Cd^{2+}. $Ca_v1.4$ variants were co-expressed with β_{2X13} and $\alpha_2\delta$-4.

$Ca_v1.4$ channels, then the outward currents in cells transfected with $Ca_v1.4\Delta ex47^{IT}$ should be reduced by known blockers of Ca_v channels such as Cd^{2+} (23) and by decreasing the chemical gradient of $NMDG^+$ across the membrane. Consistent with these predictions, Cd^{2+} abolished outward currents in cells transfected with $Ca_v1.4\Delta ex47^{IT}$ as well as the inward currents in cells expressing either WT or mutant channels (Fig. 6). To test the effects of altering the $NMDG^+$ concentration, we compared E_{rev} using extracellular solutions containing 5 or 130 mM $NMDG^+$ ($[NMDG^+]_5$ and $[NMDG^+]_{130}$, respectively, Fig. 7*A*). Although having no effect on E_{rev} of $Ca_v1.4\Delta ex47$ (66.5 ± 2.3 mV with $[NMDG^+]_5$, $n = 4$ *versus* 68.3 ± 1.4 mV with $[NMDG^+]_{130}$, $n = 4$, $p = 0.532$ by *t* test; Fig. 7, *B* and *C*), increasing extracellular $NMDG^+$ caused a positive shift in E_{rev} (31.2 ± 2.7 mV with $[NMDG^+]_5$, $n = 4$ *versus* 53.1 ± 3.6 mV with $[NMDG^+]_{130}$, $n = 3$, $p = 0.004$ by *t* test) and diminished outward currents in cells expressing $Ca_v1.4\Delta ex47^{IT}$ (Fig. 7, *B* and *C*). In addition, increasing the extracellular $[NMDG^+]$ had no effect on the permeability of Ba^{2+} *versus* $NMDG^+$ (P_{Ba}/P_{NMDG}) for $Ca_v1.4\Delta ex47$ (351.4 ± 53.4, $n = 4$, for $[NMDG^+]_5$ *versus* 391.7 ± 36.9, $n = 4$, for $[NMDG^+]_{130}$, $p = 0.558$ by *t* test) but significantly increased that for $Ca_v1.4\Delta ex47^{IT}$ (27.4 ± 5.3, $n = 4$, for $[NMDG^+]_5$ *versus* 133.4 ± 37.0, $n = 3$, for $[NMDG^+]_{130}$, $p = 0.020$ by *t* test). We further assessed the effect of IT on selectivity of $Ca_v1.4\Delta ex47$ by measuring E_{rev} and P_{Ba}/P_x under other bi-ionic conditions. With intracellular solutions containing Na^+ or K^+, IT caused a negative shift in E_{rev} and lowered P_{Ba}/P_x (Fig. 8, Table 3). Taken together, these results signified a reduction in the ionic selectivity of $Ca_v1.4\Delta ex47^{IT}$ compared with WT channels.

Although smaller for $Ca_v1.4$+ex47 than for $Ca_v1.4\Delta ex47$ (Fig. 1*C*, Table 1) the effects of IT on E_{rev} were, nevertheless, not reported for $Ca_v1.4$+ex47 in a previous study (12). A key difference was in the choice of auxiliary subunits (β_{2X13} and $\alpha_2\delta$-4, this study) *versus* β_3 or β_{2A} and $\alpha_2\delta$-1 (12)). Therefore, we tested the impact of IT on the $Ca_v1.4$ variants containing β_{2A} and $\alpha_2\delta$-1. Consistent with the previous study, IT caused a large negative shift in V_h in these experiments. Although the mutation strongly reduced current densities of $Ca_v1.4\Delta ex47$ + β_{2A} + $\alpha_2\delta$-1, IT did not affect E_{rev} (Fig. 9, *A–C*, Table 1). Thus, the identity of the auxiliary β and $\alpha_2\delta$ subunits critically determines the effects of IT on selectivity of $Ca_v1.4$.

Discussion

Our study provides new insights about how IT affects the biophysical properties of $Ca_v1.4$. First, we show that IT produces a large negative shift in voltage-dependent activation of $Ca_v1.4$ channels containing the major auxiliary Ca_v subunits in the retina, β_{2X13} and $\alpha_2\delta$-4 (Figs. 1 and 3, Table 1), as well as $Ca_v1.4$ channels comprised of other auxiliary subunits (Fig. 9, Table 1, and see Ref. 12). Second, deletion of exon 47

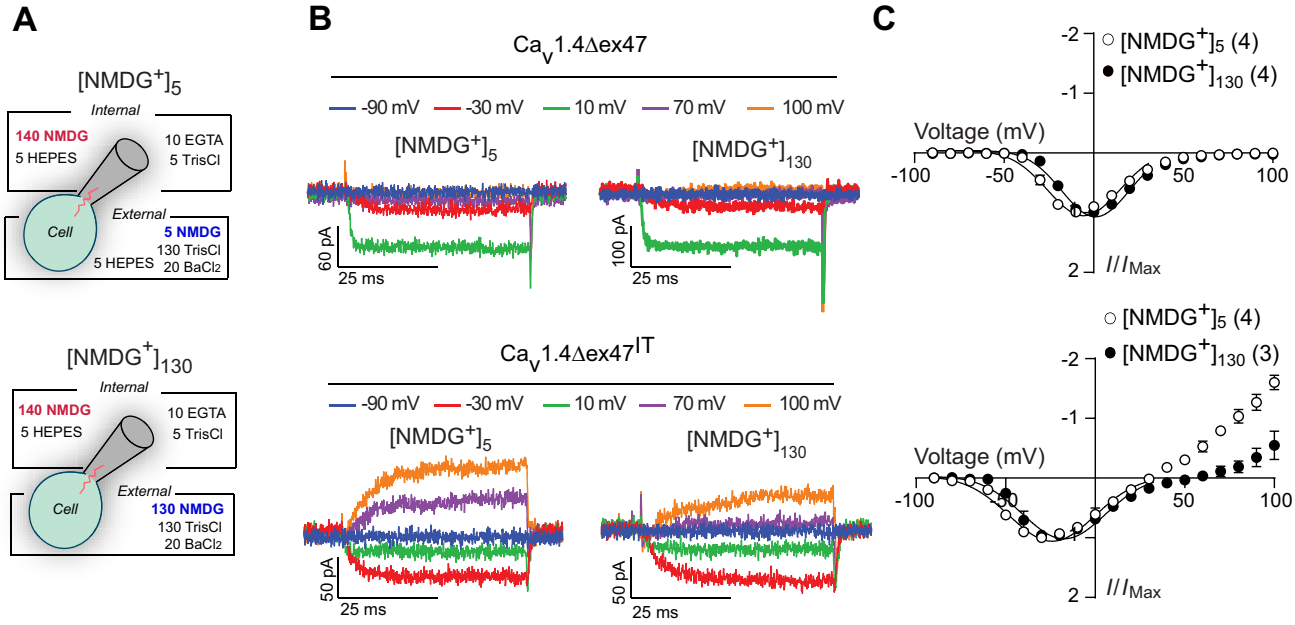

Figure 7. Increasing $NMDG^+$ in the extracellular recording solution minimizes alterations in E_{rev} and outward currents caused by IT mutation. *A*, schematic showing composition of $[NMDG]_5$ and $[NMDG]_{130}$ recording solutions. *B* and *C*, representative current traces evoked by 50-ms pulses from −100 mV to the indicated voltages (*left*) and I-V plots (*right*) in cells transfected with $Ca_v1.4\Delta ex47$ (*top*) or $Ca_v1.4\Delta ex47^{IT}$ (*bottom*). I/I_{Max} represents I_{Ba} normalized to peak inward current amplitude. $Ca_v1.4$ variants were co-expressed with β_{2X13} and $\alpha_2\delta$-4.

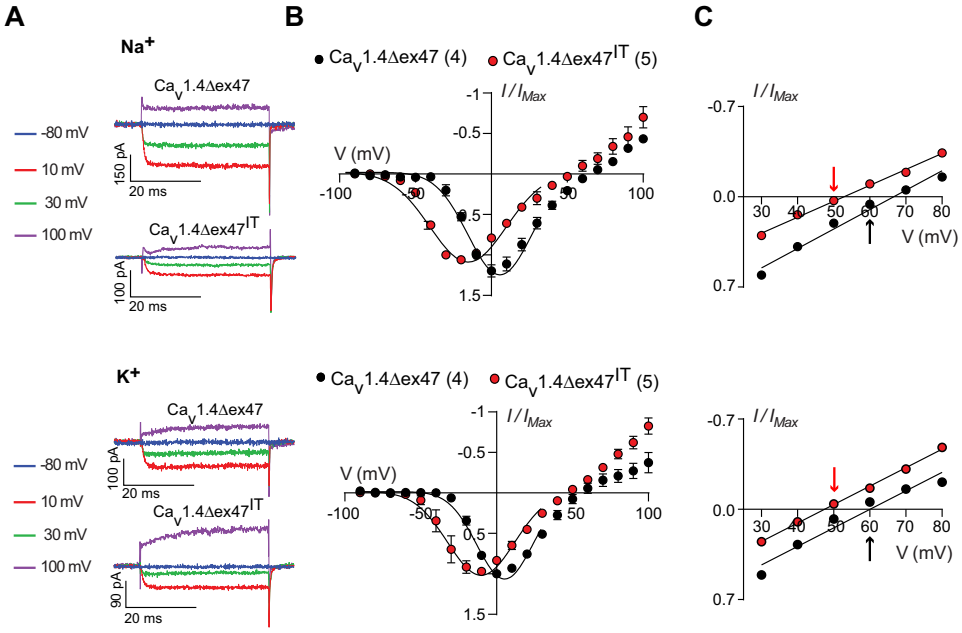

Figure 8. IT impairs selectivity of $Ca_v1.4\Delta ex47$. *A*, representative current traces evoked by 50-ms pulses from −100 mV to the indicated voltages. *B*, I-V plots in cells transfected with $Ca_v1.4\Delta ex47$ or $Ca_v1.4\Delta ex47^{IT}$. I/I_{max} represents I_{Ba} normalized to peak inward current amplitude. *C*, expanded view of I-V plots in *B* with E_{rev} indicated by *arrows* for $Ca_v1.4\Delta ex47$ (*black*) or $Ca_v1.4\Delta ex47^{IT}$ (*red*). Data were fit by linear regression. Intracellular solution contained 140 mM Na^+ (*top panels*) or K^+ (*bottom panels*). $Ca_v1.4$ variants were co-expressed with β_{2X13} and $\alpha_2\delta$-4.

exacerbates the gain of function effects of IT: $Ca_v1.4\Delta ex47^{IT}$ activates at more negative voltages and exhibits stronger voltage-dependent alterations in the kinetics of activation and deactivation than $Ca_v1.4+ex47^{IT}$ (Figs. 1–4, Tables 1 and 2). Third, IT weakens the selectivity of $Ca_v1.4$ for Ba^{2+} in a manner that varies with the identity of the auxiliary β and $\alpha_2\delta$ subunits (Figs. 1, 3, and 9, Tables 1 and 3). Our findings highlight the importance of splice variation and auxiliary subunit composition as potential modifiers of disease-causing mutations affecting Ca_v channels.

Conserved role of Ile-745 in activation gating

The S5 and S6 pore-lining helices give rise to the selectivity filter (2), with the four S6 helices (IS6–IVS6) converging at the intracellular side of the membrane in the closed state of the

Table 3

Parameters for monovalent and Ba^{2+} permeability for $Ca_v1.4\Delta ex47$ and $Ca_v1.4\Delta ex47^{IT}$

E_{rev} and P_{Ba}/P_x were determined from data shown in Figs. 7 and 8 and from equations described under "Experimental procedures," p values were determined by unpaired t tests. Intracellular solutions contained 140 mM $NMDG^+$, Na^+, or K^+. Significance was determined by Student's t test.

E_{rev} (mV)	$Ca_v1.4\Delta ex47$	$Ca_v1.4\Delta ex47^{IT}$	p Value
$NMDG^+$	66.5 ± 2.3	31.2 ± 2.7	<0.001
Na^+	65.5 ± 1.6	51.0 ± 2.7	0.004
K^+	60.9 ± 3.4	50.8 ± 3.1	0.064
P_{Ba}/P_x			
$NMDG^+$	351.4 ± 53.4	31.2 ± 2.7	0.0009
Na^+	316.6 ± 34.6	113.8 ± 19.1	0.0009
K^+	243.7 ± 58.8	116.2 ± 28.4	0.074

channel (2). Ile-745 of $Ca_v1.4$ corresponds to Ile-781 in IIS6 of $Ca_v1.2$, which lies in a cluster of hydrophobic residues (Leu-779–Ala-782, LA**I**A) in the S6 bundle-crossing region that are conserved among Ca_v1 and Ca_v2 channels (24). Disruptive mutations of these residues also cause hyperpolarizing shifts in activation and slowing of deactivation of $Ca_v1.2$ and $Ca_v2.3$ (20, 25). Our study is the first to show that the IT mutation causes similar effects on $Ca_v1.4$. Based on the correlation of their hydrophobicity and the negative shift in V_h (20, 25), the distal S6 residues are likely buried within a hydrophobic environment in the closed channel and become exposed to the aqueous milieu upon pore opening. By analogy to the model of $Ca_v1.2$ (26), contacts between Ile-745 with a corresponding hydrophobic residue in IIIS6 may stabilize helix-helix interactions, which support the closed conformation in $Ca_v1.4$, and are disrupted by the IT mutation.

Functions of exon 47 in regulating the impact of IT on $Ca_v1.4$ activation

Exon 47 encodes the initial 47 amino acids of the CTM, a modular domain present in both $Ca_v1.4$ and $Ca_v1.3$ that interacts with a region in the proximal C-terminal domain (10, 17, 27). The CTM nearly abolishes CDI of $Ca_v1.4$ by competing with calmodulin (CaM) for binding to the channel (10, 17). Deletion of the CTM enables CDI by allowing CaM binding to the channel, but also causes a negative shift in V_h (10). In $Ca_v1.4$, exon 47 is critical for the modulatory function of the CTM in that $Ca_v1.4\Delta ex47$ exhibits similar alterations in V_h and CDI as those caused by deletion of the entire CTM (16, 18). Our findings that IT and deletion of exon 47 are additive with respect to hyperpolarizing V_h (Table 1) suggest distinct mechanisms by which Ile-745 and the CTM facilitate activation. In $Ca_v1.3$, deletion of the CTM leads to stronger pairing of voltage sensor charge movement and channel opening (28). In $Ca_v2.3$, the IIS4-S5 loop and the cytoplasmic end of IIS6 are thought to functionally interact in the activation pathway (see Ref. 29). In $Ca_v1.4$, partial deletion of exon 47 might disinhibit such intramolecular interactions, allowing IT to more freely destabilize closed channels and promote channel opening at more negative voltages than in channels with a complete CTM. Interactions of S4–S5 with S6 have been studied by homology modeling and molecular dynamics simulations of K_v channels (30). Similar approaches would be useful in dissecting the relationships of the corresponding regions, and of the CTM, with respect to activation gating of $Ca_v1.4$.

The effect of IT on hyperpolarizing V_h, whereas decreasing the peak current density of $Ca_v1.4\Delta ex47$ (Table 1), parallels the effect of the S218L migraine-causing mutation in $Ca_v2.1$ expressed in HEK293 cells. In the latter case, the reduction in current density was determined to be an artifact of overexpression and related to a reduction in the number of functional channels in the membrane rather than changes in unitary current amplitudes (31). Because IT did not affect the total or cell-surface levels of $Ca_v1.4\Delta ex47$ protein (Fig. 5), the reduced current density of $Ca_v1.4\Delta ex47^{IT}$ could result from a decrease in single channel conductance, and/or the functionality of the mutant channels within the membrane. Alternatively, the extremely negative activation properties of $Ca_v1.4\Delta ex47^{IT}$ could have compromised cell health such that outward leak currents compromised I_{Ba} amplitudes and caused the negative shift in E_{rev}. This scenario seems unlikely given that IT reduced current density but did not produce outward currents or alterations in E_{rev} in $Ca_v1.4\Delta ex47$ channels containing β_{2A} and $\alpha_2\delta$-1 (Fig. 9, Table 1). Single channel recordings will be necessary to fully uncover the impact of IT on the elementary properties of $Ca_v1.4\Delta ex47$.

Effects of IT on the ion selectivity of $Ca_v1.4\Delta ex47$

The exquisite selectivity of Ca_v channels is largely determined by Ca^{2+} binding with high affinity to the selectivity filter (32, 33). Thus, the increased permeability of Na^+, K^+, and particularly $NMDG^+$ caused by a mutation outside of the selectivity filter was unexpected. However, in the absence of Ca^{2+}, Na^+ and large organic cations such as tetramethylammonium are capable of permeating Ca_v1 channels (34). These results suggest that the pore of Ca_v channels is at least 6 Å in diameter, an interpretation that has been verified in structural analyses (2, 35). Indeed, despite being a relatively large cation (~6.4 Å wide × 12 Å long; ~7.3 Å mean diameter (36)), $NMDG^+$ can permeate $Ca_v1.2$ channels containing pore mutations (37) and $Ca_v1.3$ channels exposed to the dihydropyridine agonist FPL 64176 (FPL) (21). Functional interactions between the selectivity filter and the inner S6 helix bundle are involved in K_v channel gating transitions (38) and may be conserved among Ca_v channels. For example, CaM binding to the cytoplasmic domain promotes conformational changes in the selectivity filter of Ca_v1 channels that lead to CDI (39). Thus, IT could alter positioning of IIS6 and its contributions to the Ca^{2+} (or Ba^{2+}) binding affinity within the selectivity filter, allowing monovalent ions including $NMDG^+$ and Na^+ to permeate even in the presence of significant extracellular concentrations of Ba^{2+}.

Our findings that impaired selectivity was specific to IT mutant channels containing β_{2X13} and $\alpha_2\delta$-4 explain why previous analyses did not uncover any alteration in selectivity in these channels containing β_{2A} and $\alpha_2\delta$-1 (12). Unlike β_{2A}, β_{2X13} lacks exon 7B, which causes increased voltage-dependent inactivation of $Ca_v1.4$ (5). Although it is unclear how this difference could affect ion selectivity of the IT mutant channels, there is evidence that structural alterations in $\alpha_2\delta$ could affect the permeation properties of Ca_v channels. For example, CACHD1 is

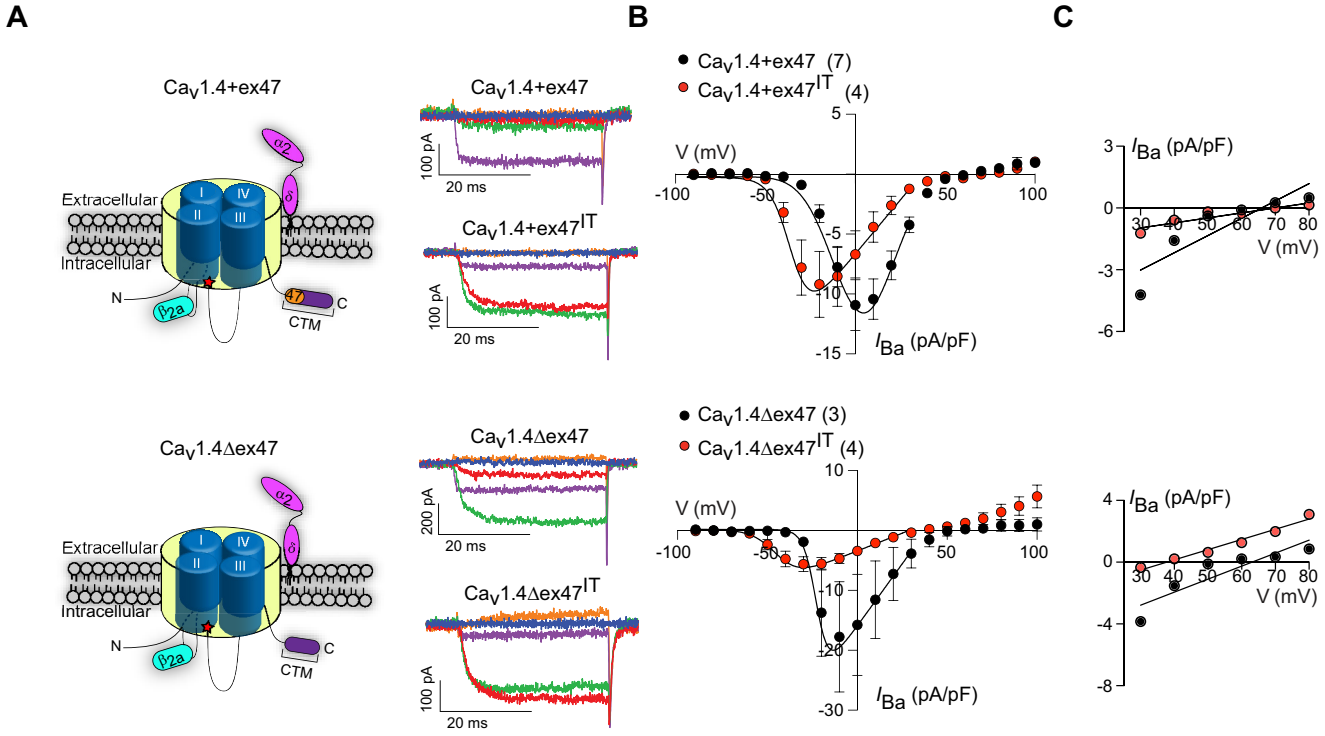

Figure 9. IT does not alter selectivity in $Ca_v1.4$ channels containing $\beta_{2A}\delta$ and $\alpha_2\delta$-1. *A,* schematics of $Ca_v1.4$ (*left*). Representative current traces evoked by 50-ms pulses from −100 mV to the indicated voltages (*right*). *B,* I-V plots in cells transfected with $Ca_v1.4$+ex47, $Ca_v1.4$+ex47^{IT}, $Ca_v1.4\Delta$ex47, or $Ca_v1.4\Delta$ex47^{IT}. I_{Ba} (pA/pF) represents I_{Ba} normalized to peak inward current amplitude. *C,* expanded view of I-V plot in *B*. Data were fit by linear regression. Extracellular and intracellular solutions were the same as those used in Figs. 1–4.

an $\alpha_2\delta$-like protein that has a disrupted metal-ion adhesion site that is critical for structural and functional interactions of $\alpha_2\delta$ with the channel (2, 40, 41). When co-expressed with $Ca_v2.2$, CACHD1 impairs the ion selectivity of $Ca_v2.2$ (42). In the cryo-EM structure, $\alpha_2\delta$-1 forms multiple extracellular contacts with $Ca_v1.1$ including the extended loops between S5 and P1 helices in domains II and III (2). The L5 loops of each of the 4 domains form a domed window above the selectivity filter that direct Ca^{2+} ions into the pore (2). Differences in how $\alpha_2\delta$ variants may interact with these extracellular sites, in concert with those produced by β subunits at intracellular sites, could determine the impact of IT on selectivity in the context of $Ca_v1.4$.

Significance for visual phenotypes of $Ca_v1.4$ channelopathies

CSNB2 is a nonprogressive retinal disorder with variable clinical features including reduced visual acuity, myopia, and nystagmus (43). A hallmark feature of this disorder is a reduced b-wave in electroretinograms, which is consistent with a defect in transmission from photoreceptors to second-order bipolar neurons (43, 44). Of the numerous CSNB2 mutations affecting *Cacna1f,* the IT mutation causes the most severe form of visual impairment (45). Despite the reduced current density of $Ca_v1.4\Delta$ex47^{IT} in our experiments, the mutation enabled significant inward I_{Ba} at voltages negative to the activation thresholds of WT channels (Fig. 3*C*). Due to charge screening effects (46), our use of 20 mM Ba^{2+} in the external recording solutions would cause activation voltages ~20 mV more positive than those expected in the retina; however, the relative differences in the voltage-dependent properties of the WT and IT mutant channels should be preserved under our recording conditions. Even in the presence of reduced current density, the negative shift in V_h and slow deactivation of $Ca_v1.4\Delta$ex47^{IT} would lead to aberrant Ca^{2+} influx during light-dependent hyperpolarization of photoreceptors, thus degrading the fidelity of visual transmission to second-order neurons. However, our study also raises the possibility that the aberrant conductance of monovalent cations by $Ca_v1.4\Delta$ex47^{IT} could lead to alterations in the excitability of photoreceptors that could lead to degenerative changes. Photoreceptor degeneration, as well as altered retinal ganglion cell activity and morphological and functional defects in photoreceptor synapses, are characteristic of an IT knock-in mouse line (47–50). However, $Ca_v1.4$ splice variants lacking exon 47, although abundant in human and monkey retina, are conspicuously absent from mouse retina (16). An understanding of the pathological consequences of $Ca_v1.4\Delta$ex47^{IT} could therefore benefit from analyses of the mutant channels in human stem-cell derived photoreceptors in the context of retinal organoids (51).

Experimental procedures

cDNAs and molecular biology

The following cDNAs were used: $Ca_v1.4$ (GenBank AF201304), β_{2A} (GenBank AF465485), β_{2X13} (GenBank NM_053851), $\alpha_2\delta$-1

(GenBank M86621), and $\alpha_2\delta$-4 (GenBank NM_172364) in pcDNA3.1. The construct encoding $Ca_v1.4\Delta ex47$ was described previously (16). To incorporate the IT mutation into $Ca_v1.4$ ($Ca_v1.4+ex47^{IT}$ and $Ca_v1.4\Delta ex47^{IT}$), the upstream and downstream cDNA regions flanking the codon corresponding to I756 were amplified with Q5 High-Fidelity DNA polymerase (New England Biolabs) using $Ca_v1.4+ex47$ as the template and primers incorporating the mutation. PCR products were digested with DpnI, column purified, and cloned into $Ca_v1.4+ex47$ and $Ca_v1.4\Delta ex47$ between AgeI and ClaI with the NEBuilder HiFi DNA Assembly kit (New England Biolabs) following the manufacturer's protocol. All constructs were verified by DNA sequencing before use.

Cell culture and transfection

Human embryonic kidney (HEK) 293 cells transformed with SV40 T antigen (HEK293T, CRL-3216, RRID:CVCL_0063; ATCC*)* were cultured in Dulbecco's modified Eagle's medium (Life Technologies, Grand Island, NY) with 10% fetal bovine serum (Atlantic Biologicals) at 37 °C in 5% CO_2. Cells were not used after they were passaged 15 times. At 70–80% confluence, the cells were co-transfected with cDNAs encoding human $Ca_v1.4$ α_1 (1.8 μg; $Ca_v1.4+ex47$, $Ca_v1.4+ex47^{IT}$, $Ca_v1.4\Delta ex47$, or $Ca_v1.4\Delta ex47^{IT}$), β_{2A} or β_{2X13} (0.6 μg), $\alpha_2\delta$-4 or $\alpha_2\delta$-1 (0.6 μg), and enhanced GFP in pEGFP-C1 (0.1 μg) using FuGENE 6 transfection reagent (Promega) according to the manufacturer's protocol. In some experiments, cells were co-transfected with a plasmid encoding SK-1 Ca^{2+}-activated K^+ channel (0.1 μg) in an effort to reduce toxicity (there were no differences in results obtained in cells transfected with or without SK-1 and thus data were combined). Cells treated with the transfection mixture were incubated at 37 °C for 24 h. After 24 h, cells were incubated at 30 °C for at least 24 h prior to whole-cell patch clamp recordings.

For Western blotting and cell-surface biotinylation assays, HEK293T cells were transfected using Lipofectamine 3000 reagent (Life Technologies). Plasmid DNA ($Ca_v1.4\Delta ex47$ or $Ca_v1.4\Delta ex47^{IT}$ (1.8 μg), β_{2X13}, and $\alpha_2\delta$-4 (0.6 μg each)) was diluted in Opti-MEM (50 μl, Life Technologies) and 4 μl of P3000 reagent. This was added to a mixture of Opti-MEM (50 μl) and Lipofectamine 3000 reagent (3 μl) and incubated for 10 min at room temperature. The DNA mixture was added incubated with the cells for 24 h at 37 °C in 5% CO_2 after which the cell culture medium was replaced with fresh medium.

Electrophysiology

Whole-cell patch clamp recordings were performed at room temperature between 48 and 72 h after transfection. Data were obtained under voltage-clamp with an EPC-9 patch clamp amplifier operated by Patchmaster software (HEKA Elektronik). The composition of recording solutions contained as follows (in mM): for Figs. 1–4 and 9, external solution contained NMDG (140), $BaCl_2$ (20), and $MgCl_2$ (1); internal solution contained NMDG (140), HEPES (10), $MgCl_2$ (2), Mg-ATP (2), and EGTA (5). For Fig. 6, Cd^{2+} (100 μM) was added to the external solution; pH was adjusted to 7.3 with methanesulfonic acid. For Fig. 7, the external solution contained Tris (130), NMDG (5 or 130), and $BaCl_2$ (20); internal solution contained NMDG (140), EGTA (10), HEPES (5), Tris (5); pH was adjusted to 7.3 with methanesulfonic acid. For Fig. 8, the external solution contained TEA-Cl (130), $BaCl_2$ (20), HEPES (5), pH 7.3, with TEA-OH); internal solution contained KCl or NaCl (140 mM), EGTA (5), HEPES (5), Tris (5), pH 7.3, with KOH or NaOH. Pipette resistances were typically 2-6 megaohms in the bath solution, and series resistance compensated up to 70%. Leak subtraction was conducted using a P/-4 protocol.

To measure current density, I_{Ba} was evoked by 50-ms pulses from a holding voltage of −100 mV to various voltages and normalized to the cell capacitance. I-V data were fitted with the Boltzmann equation: $I = G_{max} \times (V_m - E_{rev})/(1 + exp(V_h - V_m)/k$, where I is the measured current at each test voltage (V_m), V_h is the voltage of half-maximal activation, k is the slope factor, and G_{max} is the maximal conductance. Peak current density was determined by dividing the maximal I_{Ba} by the cell capacitance. Kinetic parameters for I_{Ba} activation (τ_{act}) and deactivation (τ_{deact}) were obtained by fitting the test current and tail current, respectively, with a single exponential function ($y_0 + A$ (exp($-t/\tau$)), where y_0 is the offset (asymptote), t is time, τ is the time constant, and A is the amplitude. The voltage-dependence of τ_{act} and τ_{deact} was described by: $y_0 + A$ (exp($-v/v$)), where y_0 is the asymptote, v is voltage, v is the voltage constant, and A is the amplitude. Relative permeability of Ba^{2+} *versus* different monovalent cations (x) was calculated as: $P_{Ba}/P_x = [x]_i/4[Ba^{2+}]_o \times \exp(E_{rev}F/RT)\{1 + \exp(E_{rev}F/RT)\}$. Data were analyzed offline with Igor Pro (Wavemetrics) or Origin Pro (OriginLab Corporation) software. Statistical analysis and preparation of graphs were performed using GraphPad Prism software. The data were initially analyzed for normality using the Shapiro–Wilk or D'Agostino-Pearson omnibus test. For parametric data, significant differences were determined by Student's t test. For nonparametric data, Mann-Whitney test was used. Significant differences in the curve fits of τ_{act} and τ_{deact} *versus* voltage relationships were determined by F tests. Data were incorporated into figures using GraphPad and Adobe Illustrator software. Unless otherwise indicated, averaged data represent mean ± S.E. from at least 3 independent transfections.

Biochemical analysis of cell-surface $Ca_V1.4$ protein

Transfected HEK293T cells were subject to cell-surface biotinylation and Western blotting as described previously (52). Cell-surface proteins were biotinylated according to the manufacturer's protocol. Briefly, cells were washed with ice-cold PBS (PBS, in mM: 2.5 KCl, 136 NaCl, 1.5 KH_2PO_4-Na_2HPO_4 6.5, pH 7.4), prior to incubation with sulfo-NHS-SS-biotin (Thermo Scientific) for 30 min at 4 °C. The cells were then incubated with biotin quenching solution (in mM: 50 glycine, 2.5 $CaCl_2$, 1 $MgCl_2$, pH 7.4), scraped off the plate in PBS, pelleted by centrifugation, and resuspended in lysis buffer containing in mM: 150 NaCl, 25 Tris–HCl, pH 7.6, with 1% Nonidet P-40, 1% sodium deoxycholate, 0.1% SDS, and 0.5 phenylmethylsulfonyl fluoride and other protease

inhibitors. After 10 min on ice, cell lysates were subject to centrifugation (16,000 × *g* for 10 min at 4 °C) and biotinylated proteins recovered with NeutrAvidin gel. The bound proteins were eluted in SDS-PAGE sample buffer (in mM: 58 Tris-Cl, 50 DTT, with 1.7% SDS, 5% glycerol, 0.002% bromphenol blue, pH 6.8) and subject to electrophoresis using Novex™ WedgeWell™ 4–20% Tris glycine gel (Invitrogen) and transfer to nitrocellulose blotting membranes.

For Western blotting, the membranes were incubated in blocking buffer containing milk (5%) in TBS-T (100 mM Tris–HCl, 0.15 M NaCl, 0.05% Tween 20) followed by incubation with the following antibodies diluted in blocking buffer: $Ca_V1.4$ (1:4,000 (48)); Na^+/K^+ ATPase (1:700, Developmental Studies Hybridoma Bank, University of Iowa, RRID:AB_2314847), GAPDH (1:10,000; Cell Signaling catalog number 14C10). Horseradish peroxidase (HRP)-conjugated secondary antibodies used were anti-rabbit HRP (1:3000; GE Healthcare catalog number NA934-1ML) and anti-mouse HRP (1:3000; GE Healthcare catalog number NA931V) followed by chemiluminescent detection (Thermo Scientific; SuperSignal West Pico catalog number 34080). The Western blotting signals were visualized with the Odyssey Fc Imaging System (LI-COR). The results shown were obtained from at least 3 independent experiments. Densitometric analysis was performed with Image Studio Lite software (LI-COR).

Data availability

All data relevant to this work are contained within this manuscript or available upon request.

Author contributions—B. W. and A. L. conceptualization; B. W. and A. L. data curation; B. W. software; B. W., J. A. L., and A. L. formal analysis; B. W., J. W. M., and A. L. funding acquisition; B. W., J. W. M., and A. L. validation; B. W., J. A. L., and A. L. investigation; B. W. methodology; B. W. and A. L. writing-original draft; B. W., J. A. L., J. W. M., and A. L. writing-review and editing; J. W. M. and A. L. resources; A. L. supervision; A. L. project administration.

Funding and additional information—This work was supported by National Institutes of Health Grants R01-EY026817 (to A. L.), F31-EY026477 (to B. W.), and F32-EY029953 (to J. W. M.), University of Iowa Neuroscience Training Program Grant T32 NS007421, University of Iowa's Bioscience Academy Grant R25GM058939, and University of Iowa Interdisciplinary Training Program in Pain Research Grant T32 NS045549. The content is solely the responsibility of the authors and does not necessarily represent the official views of the National Institutes of Health.

Conflict of interest—The authors declare that they have no conflicts of interest with the contents of this article.

Abbreviations—The abbreviations used are: CSNB2, congenital stationary night blindness type 2; CaM, Calmodulin; CDI, Ca^{2+}-dependent inactivation; CTM, C-terminal automodulatory domain; E_{rev}, reversal potential; IT, I745T mutation; I_{Ba}, Ba^{2+} current; *I-V*, current-voltage; τ_{act}, activation time constant; τ_{deact}, deactivation time constant; *v*, voltage constant; NMDG, *N*-methyl-d-glucamine; HRP, horseradish peroxidase; HEK, human embryonic kidney; GAPDH, glyceraldehyde-3-phosphate dehydrogenase.

References

1. Dolphin, A. C., and Lee, A. (2020) Presynaptic calcium channels: specialized control of synaptic neurotransmitter release. *Nat. Rev. Neurosci.* **21,** 213–229 CrossRef
2. Wu, J., Yan, Z., Li, Z., Qian, X., Lu, S., Dong, M., Zhou, Q., and Yan, N. (2016) Structure of the voltage-gated calcium channel $Ca_v1.1$ at 3.6 Å resolution. *Nature* **537,** 191–196 CrossRef Medline
3. Mansergh, F., Orton, N. C., Vessey, J. P., Lalonde, M. R., Stell, W. K., Tremblay, F., Barnes, S., Rancourt, D. E., and Bech-Hansen, N. T. (2005) Mutation of the calcium channel gene *Cacna1f* disrupts calcium signaling, synaptic transmission and cellular organization in mouse retina. *Hum. Mol. Genet.* **14,** 3035–3046 CrossRef Medline
4. Chang, B., Heckenlively, J. R., Bayley, P. R., Brecha, N. C., Davisson, M. T., Hawes, N. L., Hirano, A. A., Hurd, R. E., Ikeda, A., Johnson, B. A., McCall, M. A., Morgans, C. W., Nusinowitz, S., Peachey, N. S., Rice, D. S., *et al.* (2006) The nob2 mouse, a null mutation in Cacna1f: anatomical and functional abnormalities in the outer retina and their consequences on ganglion cell visual responses. *Vis. Neurosci.* **23,** 11–24 CrossRef Medline
5. Lee, A., Wang, S., Williams, B., Hagen, J., Scheetz, T. E., and Haeseleer, F. (2015) Characterization of Cav1.4 complexes ($\alpha_1$1.4, β_2, and $\alpha_2\delta$−4) in HEK293T cells and in the retina. *J. Biol. Chem.* **290,** 1505–1521 CrossRef Medline
6. Shen, Y., Heimel, J. A., Kamermans, M., Peachey, N. S., Gregg, R. G., and Nawy, S. (2009) A transient receptor potential-like channel mediates synaptic transmission in rod bipolar cells. *J. Neurosci.* **29,** 6088–6093 CrossRef Medline
7. Shiells, R. A., Falk, G., and Naghshineh, S. (1981) Action of glutamate and aspartate analogues on rod horizontal and bipolar cells. *Nature* **294,** 592–594 CrossRef Medline
8. Waldner, D. M., Bech-Hansen, N. T., and Stell, W. K. (2018) Channeling vision: $Ca_V1.4$-A critical link in retinal signal transmission. *Biomed. Res. Int.* **2018,** 7272630 CrossRef Medline
9. Hoda, J. C., Zaghetto, F., Singh, A., Koschak, A., and Striessnig, J. (2006) Effects of congenital stationary night blindness type 2 mutations R508Q and L1364H on Cav1.4 L-type Ca^{2+} channel function and expression. *J. Neurochem.* **96,** 1648–1658 CrossRef Medline
10. Singh, A., Hamedinger, D., Hoda, J. C., Gebhart, M., Koschak, A., Romanin, C., and Striessnig, J. (2006) C-terminal modulator controls Ca^{2+}-dependent gating of $Ca_v1.4$ L-type Ca^{2+} channels. *Nat. Neurosci.* **9,** 1108–1116 CrossRef Medline
11. Hoda, J. C., Zaghetto, F., Koschak, A., and Striessnig, J. (2005) Congenital stationary night blindness type 2 mutations S229P, G369D, L1068P, and W1440X alter channel gating or functional expression of Cav1.4 L-type Ca^{2+} channels. *J. Neurosci.* **25,** 252–259 CrossRef Medline
12. Hemara-Wahanui, A., Berjukow, S., Hope, C. I., Dearden, P. K., Wu, S. B., Wilson-Wheeler, J., Sharp, D. M., Lundon-Treweek, P., Clover, G. M., Hoda, J. C., Striessnig, J., Marksteiner, R., Hering, S., and Maw, M. A. (2005) A CACNA1F mutation identified in an X-linked retinal disorder shifts the voltage dependence of Cav1.4 channel activation. *Proc. Natl. Acad. Sci. U. S. A.* **102,** 7553–7558 CrossRef Medline
13. Peloquin, J. B., Rehak, R., Doering, C. J., and McRory, J. E. (2007) Functional analysis of congenital stationary night blindness type-2 CACNA1F mutations F742C, G1007R, and R1049W. *Neuroscience* **150,** 335–345 CrossRef Medline
14. Bacchi, N., Messina, A., Burtscher, V., Dassi, E., Provenzano, G., Bozzi, Y., Demontis, G. C., Koschak, A., Denti, M. A., and Casarosa, S. (2015) A new splicing isoform of Cacna2d4 mimicking the effects of c.2451insC mutation in the retina: novel molecular and electrophysiological insights. *Invest. Ophthalmol. Vis. Sci.* **56,** 4846–4856 CrossRef Medline

15. Tan, G. M., Yu, D., Wang, J., and Soong, T. W. (2012) Alternative splicing at C terminus of $Ca_v1.4$ calcium channel modulates calcium-dependent inactivation, activation potential, and current density. *J. Biol. Chem.* **287,** 832–847 CrossRef Medline
16. Haeseleer, F., Williams, B., and Lee, A. (2016) Characterization of C-terminal splice variants of $Ca_v1.4$ Ca^{2+} channels in human retina. *J. Biol. Chem.* **291,** 15663–15673 CrossRef Medline
17. Wahl-Schott, C., Baumann, L., Cuny, H., Eckert, C., Griessmeier, K., and Biel, M. (2006) Switching off calcium-dependent inactivation in L-type calcium channels by an autoinhibitory domain. *Proc. Natl. Acad. Sci. U.S.A.* **103,** 15657–15662 CrossRef Medline
18. Williams, B., Haeseleer, F., and Lee, A. (2018) Splicing of an automodulatory domain in Cav1.4 Ca(2+) channels confers distinct regulation by calmodulin. *J. Gen. Physiol.* **150,** 1676–1687 CrossRef Medline
19. Adams, P. J., Garcia, E., David, L. S., Mulatz, K. J., Spacey, S. D., and Snutch, T. P. (2009) $Ca_v2.1$ P/Q-type calcium channel alternative splicing affects the functional impact of familial hemiplegic migraine mutations: implications for calcium channelopathies. *Channels* **3,** 110–121 CrossRef Medline
20. Hohaus, A., Beyl, S., Kudrnac, M., Berjukow, S., Timin, E. N., Marksteiner, R., Maw, M. A., and Hering, S. (2005) Structural determinants of L-type channel activation in segment IIS6 revealed by a retinal disorder. *J. Biol. Chem.* **280,** 38471–38477 CrossRef Medline
21. Wang, Y., Tang, S., Harvey, K. E., Salyer, A. E., Li, T. A., Rantz, E. K., Lill, M. A., and Hockerman, G. H. (2018) Molecular determinants of the differential modulation of $Ca_v1.2$ and $Ca_v1.3$ by nifedipine and FPL 64176. *Mol. Pharmacol.* **94,** 973–983 CrossRef Medline
22. Hockerman, G. H., Johnson, B. D., Scheuer, T., and Catterall, W. A. (1995) Molecular determinants of high affinity phenylaklyamine block of L-type calcium channels. *J.Biol.Chem.* **270,** 22119–22122 CrossRef
23. Lansman, J. B., Hess, P., and Tsien, R. W. (1986) Blockade of current through single calcium channels by Cd^{2+}, Mg^{2+}, and Ca^{2+}: voltage and concentration dependence of calcium entry into the pore. *J. Gen. Physiol.* **88,** 321–347 CrossRef Medline
24. Hering, S., Zangerl-Plessl, E. M., Beyl, S., Hohaus, A., Andranovits, S., and Timin, E. N. (2018) Calcium channel gating. *Pflugers Arch.* **470,** 1291–1309 CrossRef Medline
25. Raybaud, A., Baspinar, E. E., Dionne, F., Dodier, Y., Sauve, R., and Parent, L. (2007) The role of distal S6 hydrophobic residues in the voltage-dependent gating of CaV2.3 channels. *J. Biol. Chem.* **282,** 27944–27952 CrossRef Medline
26. Hering, S., Beyl, S., Stary, A., Kudrnac, M., Hohaus, A., Guy, H. R., and Timin, E. (2008) Pore stability and gating in voltage-activated calcium channels. *Channels* **2,** 61–69 CrossRef Medline
27. Singh, A., Gebhart, M., Fritsch, R., Sinnegger-Brauns, M. J., Poggiani, C., Hoda, J. C., Engel, J., Romanin, C., Striessnig, J., and Koschak, A. (2008) Modulation of voltage- and Ca^{2+}-dependent gating of CaV1.3 L-type calcium channels by alternative splicing of a C-terminal regulatory domain. *J. Biol. Chem.* **283,** 20733–20744 CrossRef Medline
28. Lieb, A., Ortner, N., and Striessnig, J. (2014) C-terminal modulatory domain controls coupling of voltage-sensing to pore opening in Cav1.3 L-type Ca^{2+} channels. *Biophys. J.* **106,** 1467–1475 CrossRef Medline
29. Wall-Lacelle, S., Hossain, M. I., Sauve, R., Blunck, R., and Parent, L. (2011) Double mutant cycle analysis identified a critical leucine residue in the IIS4S5 linker for the activation of the Ca(V)2.3 calcium channel. *J. Biol. Chem.* **286,** 27197–27205 CrossRef Medline
30. Labro, A. J., Raes, A. L., Grottesi, A., Van Hoorick, D., Sansom, M. S., and Snyders, D. J. (2008) Kv channel gating requires a compatible S4-S5 linker and bottom part of S6, constrained by non-interacting residues. *J. Gen. Physiol.* **132,** 667–680 CrossRef Medline
31. Tottene, A., Pivotto, F., Fellin, T., Cesetti, T., van den Maagdenberg, A. M., and Pietrobon, D. (2005) Specific kinetic alterations of human $Ca_V2.1$ calcium channels produced by mutation S218L causing familial hemiplegic migraine and delayed cerebral edema and coma after minor head trauma. *J. Biol. Chem.* **280,** 17678–17686 CrossRef Medline
32. Ellinor, P. T., Yang, J., Sather, W. A., Zhang, J. F., and Tsien, R. W. (1995) Ca^{2+} channel selectivity at a single locus for high-affinity Ca^{2+} interactions. *Neuron* **15,** 1121–1132 CrossRef Medline
33. Yang, J., Ellinor, P. T., Sather, W. A., Zhang, J. F., and Tsien, R. W. (1993) Molecular determinants of Ca^{2+} selectivity and ion permeation in L-type Ca^{2+} channels. *Nature* **366,** 158–161 CrossRef Medline
34. McCleskey, E. W., and Almers, W. (1985) The Ca channel in skeletal muscle is a large pore. *Proc. Natl. Acad. Sci. U.S.A.* **82,** 7149–7153 CrossRef Medline
35. Tang, L., Gamal El-Din, T. M., Payandeh, J., Martinez, G. Q., Heard, T. M., Scheuer, T., Zheng, N., and Catterall, W. A. (2014) Structural basis for Ca^{2+} selectivity of a voltage-gated calcium channel. *Nature* **505,** 56–61 CrossRef Medline
36. Villarroel, A., Burnashev, N., and Sakmann, B. (1995) Dimensions of the narrow portion of a recombinant NMDA receptor channel. *Biophys. J.* **68,** 866–875 CrossRef Medline
37. Hockerman, G. H., Johnson, B. D., Abbott, M. R., Scheuer, T., and Catterall, W. A. (1997) Molecular determinants of high affinity phenylalkylamine block of L-type calcium channels in transmembrane segment IIIS6 and the pore region of the alpha1 subunit. *J. Biol. Chem.* **272,** 18759–18765 CrossRef Medline
38. Cuello, L. G., Cortes, D. M., and Perozo, E. (2017) The gating cycle of a K^+ channel at atomic resolution. *Elife* **6,** e28032 CrossRef
39. Abderemane-Ali, F., Findeisen, F., Rossen, N. D., and Minor, D. L., Jr. (2019) A selectivity filter gate controls voltage-gated calcium channel calcium-dependent inactivation. *Neuron* **101,** 1134–1149.e3 CrossRef Medline
40. Canti, C., Nieto-Rostro, M., Foucault, I., Heblich, F., Wratten, J., Richards, M. W., Hendrich, J., Douglas, L., Page, K. M., Davies, A., and Dolphin, A. C. (2005) The metal-ion-dependent adhesion site in the Von Willebrand factor: a domain of $\alpha_2\delta$ subunits is key to trafficking voltage-gated Ca^{2+} channels. *Proc. Natl. Acad. Sci. U.S.A.* **102,** 11230–11235 CrossRef Medline
41. Cassidy, J. S., Ferron, L., Kadurin, I., Pratt, W. S., and Dolphin, A. C. (2014) Functional exofacially tagged N-type calcium channels elucidate the interaction with auxiliary $\alpha2\delta$-1 subunits. *Proc. Natl. Acad. Sci. U.S.A.* **111,** 8979–8984 CrossRef Medline
42. Dahimene, S., Page, K. M., Kadurin, I., Ferron, L., Ho, D. Y., Powell, G. T., Pratt, W. S., Wilson, S. W., and Dolphin, A. C. (2018) The $\alpha2\delta$-like protein Cachd1 increases N-type calcium currents and cell surface expression and competes with $\alpha2\delta$-1. *Cell Rep.* **25,** 1610–1621.e5 CrossRef Medline
43. Boycott, K. M., Pearce, W. G., and Bech-Hansen, N. T. (2000) Clinical variability among patients with incomplete X-linked congenital stationary night blindness and a founder mutation in CACNA1F. *Can. J. Ophthalmol.* **35,** 204–213 CrossRef Medline
44. Miyake, Y., Yagasaki, K., Horiguchi, M., Kawase, Y., and Kanda, T. (1986) Congenital stationary night blindness with negative electroretinogram: a new classification. *Arch. Ophthalmol.* **104,** 1013–1020 CrossRef Medline
45. Hope, C. I., Sharp, D. M., Hemara-Wahanui, A., Sissingh, J. I., Lundon, P., Mitchell, E. A., Maw, M. A., and Clover, G. M. (2005) Clinical manifestations of a unique X-linked retinal disorder in a large New Zealand family with a novel mutation in CACNA1F, the gene responsible for CSNB2. *Clin. Exp. Ophthalmol.* **33,** 129–136 CrossRef Medline
46. Frankenhaeuser, B., and Hodgkin, A. L. (1957) The action of calcium on the electrical properties of squid axons. *J. Physiol.* **137,** 218–244 CrossRef Medline
47. Regus-Leidig, H., Atorf, J., Feigenspan, A., Kremers, J., Maw, M. A., and Brandstätter, J. H. (2014) Photoreceptor degeneration in two mouse models for congenital stationary night blindness type 2. *PLoS ONE* **9,** e86769 CrossRef Medline
48. Liu, X., Kerov, V., Haeseleer, F., Majumder, A., Artemyev, N., Baker, S. A., and Lee, A. (2013) Dysregulation of $Ca_v1.4$ channels disrupts the maturation of photoreceptor synaptic ribbons in congenital stationary night blindness type 2. *Channels* **7,** 514–523 CrossRef Medline
49. Knoflach, D., Kerov, V., Sartori, S. B., Obermair, G. J., Schmuckermair, C., Liu, X., Sothilingam, V., Garcia Garrido, M., Baker, S. A., Glosmann, M.,

Schicker, K., Seeliger, M., Lee, A., and Koschak, A. (2013) $Ca_v1.4$ IT mouse as model for vision impairment in human congenital stationary night blindness type 2. *Channels* **7,** 503–513 CrossRef Medline

50. Knoflach, D., Schicker, K., Glösmann, M., and Koschak, A. (2015) Gain-of-function nature of $Ca_v1.4$ L-type calcium channels alters firing properties of mouse retinal ganglion cells. *Channels* **9,** 298–306 CrossRef Medline
51. Clevers, H. (2016) Modeling development and disease with organoids. *Cell* **165,** 1586–1597 CrossRef Medline
52. Garza-Lopez, E., Lopez, J. A., Hagen, J., Sheffer, R., Meiner, V., and Lee, A. (2018) Role of a conserved glutamine in the function of voltage-gated Ca^{2+} channels revealed by a mutation in human CACNA1D. *J. Biol. Chem.* **293,** 14444–14454 CrossRef Medline